Digital Transportation
and Safety

REVIEW

Open Access

https://doi.org/10.48130/DTS-2023-0010
Digital Transportation and Safety **2023**, 2(2):124−138

Modeling continuous traffic flow with the average velocity effect of multiple vehicles ahead on gyroidal roads

Cong Zhai[1,2], Weitiao Wu[2*] and Yingping Xiao[1,2]

[1] *School of Transportation and Civil Engineering and Architecture, Foshan University, Foshan 528000, Guangdong, China*
[2] *School of Civil Engineering and Transportation, South China University of Technology, Guangzhou 510641, Guangdong, China*
* Corresponding author, E-mail: ctwtwu@scut.edu.cn

Abstract

In the future connected vehicle environment, the information of multiple vehicles ahead can be readily collected in real-time, such as the velocity or headway, which provides more opportunities for information exchange and cooperative control. Meanwhile, gyroidal roads are one of the fundamental road patterns prevalent in mountainous areas. To effectively control the system, it is therefore significant to explore the evolution mechanism of traffic flow on gyroidal roads under a connected vehicle environment. In this paper, we present a new continuum model with the average velocity of multiple vehicles ahead on gyroidal roads. The stability criterion and KdV-Burger equation are deduced *via* linear and nonlinear stability analysis, respectively. Solving the above KdV-Burger equation yields the density wave solution, which explores the formation and propagation property of traffic jams near the neutral stability curve. Simulation examples verify that the model can reproduce complex phenomena, such as shock waves and rarefaction waves. The analysis of the local cluster effect shows that the number of vehicles ahead and the radius information, and the slope information of gyroidal roads can exert a great influence on traffic jams. The effect of the first and second terms are positive, while the last term is negative.

Keywords: Average velocity of multiple vehicles ahead, Gyroidal roads, Continuum model, Stability, KdV-Burger equation

Citation: Zhai C, Wu W, Xiao Y. 2023. Modeling continuous traffic flow with the average velocity effect of multiple vehicles ahead on gyroidal roads. *Digital Transportation and Safety* 2(2):124−138 https://doi.org/10.48130/DTS-2023-0010

Introduction

In the past decade, car ownership has significantly increased and poses tremendous pressure on urban traffic commuting, which raises serious issues of traffic pollution, traffic noise, and traffic safety. Improvement of traffic efficiency has attracted strong interest from both industry and the scientific community. In practice, a number of external countermeasures have been applied to ease traffic congestion, such as road marking redesign and one-way traffic management. Another branch focuses on understanding the formation and propagation mechanism of traffic jams to more effectively control the traffic system, yielding a variety of traffic flow models.

Methodologically, existing traffic flow models can be grouped into microscopic traffic flow models and macroscopic traffic flow models. The research subject of the former is each vehicle, focusing on the kinetic behavior of running vehicles, which is represented by car following models[1−6] and cellular automata models[7−8]. However, a sufficiently large number of vehicles will significantly complicate model development and problem-solving. In contrast, the latter analogizes traffic flow to compressible continuous fluid, thereby establishing a partial differential equation based on speed and density. By solving this equation, the relevant dynamic behavior of traffic flow can be explored, which is represented by lattice hydrodynamics models[9−16] and continuous models[17]. Compared with microscopic models, less simulation time is required for macroscopic models to replicate the overall characteristics of traffic flow, being independent of the number of vehicles.

Macroscopic traffic flow models originated from the LWR model proposed by Lighthill & Whitham and Richards[18−20], whereas the velocities in this model are always under equilibrium, which cannot analyze various equilibrium traffic phenomena. Payne[21] presented the first high-order continuum model by replacing the relationship of equilibrium velocity and density in the LWR model with the kinetic equations of velocity, in which the velocity is allowed to deviate from the equilibrium velocity. In 1995, Daganzo[22] found that the propagation velocity of small disturbances in Payne's model was greater than the macroscopic velocity, which meant that the vehicle is restrained by the vehicles behind, and he criticized that the model violated the fundamental properties of anisotropy of traffic flow. Subsequently, Zhang[23] and Jiang et al.[24] substituted the density gradient term in previous continuum models with the velocity gradient term, and established the anisotropy of the macroscopic traffic flow model.

As an important branch of macroscopic traffic models, continuous models have gained wide attention from the scientific community. Interested readers are referred to the representative works in Table 1. Notwithstanding that, existing studies mostly focus on the kinetic behavior of traffic flow on regular roads, whereas research on continuous models on spiral roads is rare. In many rural and mountainous areas, the roads exhibit a gyroidal upward or downward pattern due to geology and geomorphology. Compared with regular roads, the force of vehicles driving on gyroidal roads is much more complicated Fig. 1. The vehicles will not only be affected by

Table 1. Representative literature on continuum models.

Authors	Characteristics	References
Mohan R, Chen R	Heterogeneous traffic flow	[25–27]
Lu S	Higher-order	[28,29]
Liu H, Cheng R	Traffic jerk effect	[30,31]
Hao L, Yu L.	Delay effect	[32,33]
Liu Z, Zhai C	Taillight effect	[34,35]
Jiao Y, Zhai C	Backward looking effect	[36,37]
Cheng R, Zhai Q	Memory effect	[38–40]
Cheng R, Wang Z	Driver's characteristics	[41,42]
Zhai C, Chen J	Slope road / Gradient highways	[43,44]
Xue Y, Liu Z	Curved road	[45,46]
Guan X, Peng G	Anticipation effect	[47,48]
Ngoduy D, Bouadi M	Stochastic continuum models	[49,50]
Wang Z, Tang T	Driver's bounded rationality	[51,52]

Fig. 1 Common gyroidal roads in China. (a) Longmen ancient road at the junction of Henan and Shanxi; (b) East line mountain road project in Fugu County, Yulin City, Shaanxi Province.

gravity but also by centripetal force. However, existing traffic flow models on gyroidal roads are mostly analyzed in the context of microscopic models[53,54]. Given the practical and theoretical significance of macroscopic models, it is imperative to propose a customized continuum model and analyze the formation and spreading mechanism of perturbation waves on gyroidal roads.

With the advance of communication technology, the connected vehicle environment is expected to become commercially available in future transportation. Under such an environment, the information of multiple vehicles ahead can be readily collected in real-time, such as the velocity or headway, which provides more opportunities for information exchange and cooperative control. On review of the literature, no study has focused on the stability characteristics of connected vehicle flow on gradient roads from the macroscopic perspective.

To effectively control the system, it is, therefore, significant to explore the evolution mechanism of traffic flow on gyroidal roads under a connected vehicle environment. This paper aims to fill these gaps and contributes to developing a new continuum model accounting for the average velocity of multiple vehicles ahead on gyroidal roads. The linear and nonlinear stability analysis of the proposed continuum model is carried out, and the corresponding stability area and the propagation mechanism of traffic density wave are obtained.

The structural organization of this paper is as follows: In the next section, a modified continuous model taking into account the average velocity effect of multiple vehicles ahead on gyroidal roads is proposed. Next, the stability criterion and correspondingly KdV-Burgers equation is deduced *via* the small perturbation method, respectively. In the penultimate section, a numerical example is carried out to verify theoretical analysis conclusions. Finally, the key conclusions are presented.

Model

In this section, we revisit the traditional model and introduce the rationale behind our proposed model. The primary notations used in this paper are listed in Table 2. In 1995, an optimal speed (OV) model was proposed by Bando et al.[55] to explore the interaction between vehicles on a single lane. The kinetic equation is described as follows:

$$\frac{dv_n}{dt} = a\left[V^{op}(\Delta x_n) - v_n\right] \tag{1}$$

The optimal velocity function in the above equation is set as follows:

$$V^{op}(\Delta x_n) = \frac{v_{\max}}{2}\left[\tanh(\Delta x_n - y_s) + \tanh(y_s)\right] \tag{2}$$

Later, Helbing & Tilch[56] found that there were unreasonable acceleration and deceleration behaviors in the above OV model. To solve the problem, they argued that the velocity difference between the preceding vehicle and the current vehicle should be considered when the velocity of the current vehicle is less than following vehicles, thereby giving the generalized force (GF) model as follows:

$$\frac{dv_n}{dt} = a\left[V^{op}(\Delta x_n) - v_n\right] + \lambda H(-\Delta v_n)\Delta v_n \tag{3}$$

Jiang et al.[57] used the GF model to simulate the starting process of the stationary vehicle and noticed that the starting wave speed of the model was too small. They argued that the velocity difference term also should be considered whether the current vehicle velocity is greater than the velocity of the preceding vehicle, yielding a full velocity difference (FVD) model, which is described as follows:

$$\frac{dv_n}{dt} = a\left[V^{op}(\Delta x_n) - v_n\right] + \lambda \Delta v_n \tag{4}$$

In the aforementioned works, vehicles are assumed to run on a regular road scene, that is, the road slope information is neglected. In many developing countries or rural mountainous areas, gyroidal road scenes are prevalent. The force of a vehicle running on gyroidal roads is much more complicated, which is not only affected by the gravity and driving force, but also by the centripetal force. Figure 2 portrays the force decomposition diagram of the vehicles running on the gyroidal road. To analyze the interaction between successive vehicles on this special road scene, Zhu & Yu[53] improved on the OV model and proposed a new traffic flow model as follows:

$$\frac{d^2 s_n}{dt^2} = a\left[V(\Delta s_n) - \frac{ds_n}{dt}\right] \tag{5}$$

The function $V(\cdot)$ is expressed as:

$$V(r\Delta\varphi_n) = \frac{r\omega_{\max} - v_{g,\max}}{2}\left[\tanh\left(r\Delta\varphi_n - y_s(\theta)\right) + \tanh\left(y_s(\theta)\right)\right] \tag{6}$$

In order to determine $\omega_{\max}$, from the centripetal force formula, we can obtain the following equation:

$$m\omega_{\max}^2 r = \mu mg\cos\theta \tag{7}$$

Furthermore:

$$\omega_{\max} = \sqrt{\frac{\mu g\cos\theta}{r}} \tag{8}$$

Substituting Eq (8) into Eq (6), we have:

Table 2. Primary notations used in the proposed model.

Symbols	Definition
n	The subscript of vehicles
a	Driver's sensitivity
v_n	The instantaneous velocity of vehicle *n*
Δx_n	The instantaneous headway of vehicle *n*
$V^{op}(\cdot)$	Optimal velocity function
$v_{\max}$	The maximum allowable driving velocity under regular road scenes
y_s	Safety distance without collisions under regular road scenes
λ	Sensitivity coefficient of the velocity difference
$H(\cdot)$	Heaviside function
s_n	Instantaneous position information of vehicle *n* on the gyroidal road, and $s_n = r\times\varphi_n$
Δs_n	Instantaneous headway information of vehicle *n* on the gyroidal road, and $\Delta s_n = r\times\Delta\varphi_n$
r	The radius of curvature, where $r = \gamma/\cos\theta$
γ	The radius of the circle
θ	Slope angle, $\theta < 0$ and $\theta > 0$ corresponding to downhill and uphill scenes respectively
$V(\cdot)$	Optimal speed function on the gyroidal road
$\omega_{\max}$	The maximum allowable angular velocity on gyroidal roads
$y_s(\theta)$	The minimum allowable safety distance on gyroidal roads, where $y_s(\theta) = y_s(1-\alpha\sin\theta)$
α	Is a constant. Here, we set it as $\alpha = 1$
$v_{g,\max}$	Maximum reduced or enhanced speed on the gyroidal road, to simplify the calculation, we set $v_{g,\max} = \sin\theta$
m	The mass of vehicles
g	Gravitational acceleration information, where we set g = 9.8 $m\cdot s^{-1}$
μ	Lateral friction coefficient
k	The adjustment coefficient; here $k = 0.1$
l	The number of vehicles ahead considered

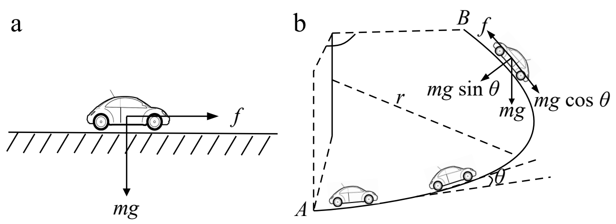

Fig. 2 Illustration of vehicle forces on different road scenes, (a) horizontal or regular road, (b) gyroidal road.

$$V(r\Delta\varphi_n) = \frac{k\sqrt{\mu gr\cos\theta} \mp \sin\theta}{2} V_0(r\Delta\varphi_n) \tag{9}$$

where $V_0(r\Delta\varphi_n) = \tanh\left(r\Delta\varphi_n - y_s(\theta)\right) + \tanh\left(y_s(\theta)\right)$.

Incorporating Eq (9) into Eq (5), and introducing the intermediate variable ω_n, then we have:

$$\frac{d\omega_n}{dt} = a\left[\frac{k\sqrt{\mu gr\cos\theta} \mp \sin\theta}{2r} V_0(r\Delta\varphi_n) - \omega_n\right] \tag{10}$$

where $\omega_n = \frac{d\varphi_n}{dt}, \frac{d\omega_n}{dt} = \frac{d^2 s_n}{dt^2}$.

With the advancements in communication technology, the information of multiple vehicles ahead can be readily collected in real-time, such as the velocity or headway, which provides more opportunities for information exchange and cooperative control[58,59]. Based on this, we introduce the effect of the average velocity of multiple vehicles ahead, and a new macroscopic traffic flow model is given:

$$\frac{d\omega_n}{dt} = a\left[\frac{k\sqrt{\mu gr\cos\theta} \mp \sin\theta}{2r} V_0(r\Delta\varphi_n) - \omega_n\right] + \lambda\left(\frac{1}{l}\sum_{m=1}^{l}\omega_{n+l} - \omega_n\right) \tag{11}$$

where $\frac{1}{l}\sum_{m=1}^{l}\omega_{n+l}(t) - \omega_n(t)$ represents the comprehensive velocity difference information between the average speed of multiple vehicles ahead and the current vehicle.

Remark 1: When $l = 1$, only the velocity difference term between the preceding vehicle and the current vehicle is considered in the proposed model, which is similar to the traditional FVD model. When $\lambda = 0$, the model collapses to Zhu & Yu's model[53]. Therefore, previous models can be regarded as a special form of the proposed model.

The headway-density equation proposed by Berg et al.[60] builds the linkage between the microscopic and the macroscopic traffic flow model:

$$r\Delta\varphi_n \approx \frac{1}{\rho} - \frac{\rho_x}{2\rho^3} - \frac{\rho_{xx}}{6\rho^4} \tag{12}$$

Similarly, the rest of the microscopic variables in Eq (11) can be converted into the following forms:

$$\begin{aligned} &\omega_n(t) \to \omega(\varphi, t), \omega_{n+l}(t) \to \omega(\varphi + l\Delta, t), \\ &V_0\left(\frac{1}{\rho}\right) \to V_e(\rho), V_0'\left(\frac{1}{\rho}\right) \to -\rho^2 V_e'(\rho) \end{aligned} \tag{13}$$

The left side term of Eq (11) can be transformed into:

$$\frac{d\omega(\varphi,t)}{dt} = \frac{\partial\omega(\varphi,t)}{\partial\varphi}\omega + \frac{\partial\omega(\varphi,t)}{\partial t}. \tag{14}$$

Similarly, Taylor expansion is carried out on the variable $\omega(\varphi + l\Delta, t)$, the following approximation can be obtained:

$$\omega(\varphi + l\Delta, t) = \omega(\varphi, t) + \omega' l\Delta + \frac{1}{2}\omega'' l^2\Delta^2 \tag{15}$$

Incorporating Eqs (12)–(15) into Eq (11) and sorting it, the following new continuous model can be obtained:

$$\begin{cases} \frac{\partial\rho}{\partial t} + \omega\frac{\partial\rho}{\partial\varphi} + \rho\frac{\partial\omega}{\partial\varphi} = 0 \\ \frac{\partial\omega}{\partial t} + \left(\omega - \frac{l+1}{2}\lambda\Delta\right)\frac{\partial\omega}{\partial\varphi} = a\left(\frac{k\sqrt{\mu gr\cos\theta} \mp \sin\theta}{2r} V_e(\rho) - \omega\right) + \\ \quad \frac{(l+1)(2l+1)}{12}\lambda\omega''\Delta^2 + a\frac{k\sqrt{\mu gr\cos\theta} \mp \sin\theta}{2r} V'_e(\rho)\left(\frac{\rho_\varphi}{2\rho} + \frac{\rho_{\varphi\varphi}}{6\rho^2}\right) \end{cases} \tag{16}$$

Linear stability analysis

For ease of the subsequent discussion, we convert Eq (16) into the following matrix form:

$$\frac{\partial \vec{U}}{\partial t} + \vec{A}\frac{\partial \vec{U}}{\partial \varphi} = \vec{E} \tag{17}$$

where $\vec{U} = \begin{pmatrix} \rho \\ \omega \end{pmatrix}$, $\vec{A} = \begin{bmatrix} \omega & \rho \\ 0 & \omega - \frac{l+1}{2}\lambda l \Delta \end{bmatrix}$,

$$\vec{E} = \begin{bmatrix} 0 \\ a\left(\frac{k\sqrt{\mu g r}\cos\theta \mp \sin\theta}{2r}V_e(\rho) - \omega\right) + \frac{(l+1)(2l+1)}{12}\lambda\omega''\Delta^2 \\ +a\frac{k\sqrt{\mu g r}\cos\theta \mp \sin\theta}{2r}V'_e(\rho)\left(\frac{\rho_x}{2\rho} + \frac{\rho_{xx}}{6\rho^2}\right) \end{bmatrix}.$$

In order to obtain the eigenvalues of the above equations, matrix A must satisfy the following eigenvalues:

$$|\kappa I - A| = 0 \tag{18}$$

By solving Eq (18), we can obtain the characteristic solution of the above determinant:

$$\kappa_1 = \omega, \quad \kappa_2 = \omega - \frac{r+1}{2}\lambda\Delta \tag{19}$$

Since $\lambda, \Delta > 0$, then the macroscopic velocity of the traffic flow ω exceeds the characteristic velocity $\kappa_i (i = 1, 2)$, which means that the new traffic flow model has anisotropic characteristics.

In what follows, we carried out the linear stability analysis on the proposed continuum model *via* the small perturbation method to obtain the corresponding stability conditions. For a start, a small disturbance is injected into the initial equilibrium state, and then:

$$\begin{pmatrix} \rho \\ \omega \end{pmatrix} = \begin{pmatrix} \rho_0 \\ \omega_0 \end{pmatrix} + \sum \begin{pmatrix} \hat{\rho}_k \\ \hat{\omega}_k \end{pmatrix} \exp(ik\varphi + \delta_k t) \tag{20}$$

where (ρ_0, ω_0) is the steady-state solution for Eq (16), $(\hat{\rho}_k, \hat{\omega}_k)$ is the small perturbation, and k and $\delta_k$represents the wave number and frequency of the waves, respectively.

Combining Eq (20) with Eq (16) and linearizing, and neglecting the higher-order nonlinear terms, then we have:

$$\begin{cases} (\delta_k + \omega_0 ik)\hat{\rho}_k + \rho_0 ik\hat{\omega}_k = 0 \\ \left(1 + \frac{ik}{2\rho_0} + \frac{(ik)^2}{6\rho_0^2}\right)\frac{k\sqrt{\mu g r}\cos\theta \mp \sin\theta}{2r}aV'_e(\rho_0)\hat{\rho}_k - \\ \left[a + \delta_k + \left(\omega_0 - \frac{l+1}{2}\lambda\Delta\right)ik - \frac{(l+1)(2l+1)}{12}\lambda\Delta^2(ik)^2\right]\hat{\omega}_k = 0 \end{cases} \tag{21}$$

In order to obtain the non-zero solutions of $\hat{\rho}_k$ and $\hat{\omega}_k$, the determinant of the coefficient matrix of the above formula must be equal to zero, then we have the following quadratic equation:

$$(\delta_k + \omega_0 ik)^2 + (\delta_k + \omega_0 ik)\left(a - \frac{l+1}{2}\lambda\Delta ik - \frac{(l+1)(2l+1)}{12}\lambda\Delta^2(ik)^2\right) + \left(1 + \frac{ik}{2\rho_0} + \frac{(ik)^2}{6\rho_0^2}\right)\frac{k\sqrt{\mu g r}\cos\theta \mp \sin\theta}{2r}a\rho_0 V'_e(\rho_0)ik = 0 \tag{22}$$

Furthermore, to determine the value of δ_k, it is expanded into a power series, i.e. $\delta_k = \delta_1 ik + \delta_2(ik)^2 + \ldots$. To ensure the equation holds after bringing the power series into Eq (22), then the first and second order coefficients terms of ik in the above formula must always be zero, then we have:

$$\begin{cases} \delta_1 + \omega_0 + \frac{k\sqrt{\mu g r}\cos\theta \mp \sin\theta}{2r}\rho_0 V'_e(\rho_0) = 0 \\ (\delta_1 + \omega_0)^2 + a\delta_2 - \frac{l+1}{2}(\delta_1 + \omega_0)\lambda\Delta + \frac{k\sqrt{\mu g r}\cos\theta \mp \sin\theta}{4r}aV'_e(\rho_0) = 0 \end{cases} \tag{23}$$

Solving the above formula, we can see that δ_1 and δ_2 are respectively:

$$\begin{cases} \delta_1 = -\omega_0 - \frac{k\sqrt{\mu g r}\cos\theta \mp \sin\theta}{2r}\rho_0 V'_e(\rho_0) \\ \delta_2 = -\frac{1}{a}\left(\frac{k\sqrt{\mu g r}\cos\theta \mp \sin\theta}{2r}\rho_0 V'_e(\rho_0)\right)^2 - \frac{k\sqrt{\mu g r}\cos\theta \mp \sin\theta}{4r}V'_e(\rho_0) \\ \quad - \frac{k\sqrt{\mu g r}\cos\theta \mp \sin\theta}{4ar}(l+1)\lambda\Delta\rho_0 V'_e(\rho_0) \end{cases} \tag{24}$$

According to the stability theory, we can see that the new continuum model is stable when $\delta_2 > 0$, then we can obtain the following stability conditions, specifically:

$$a > -(l+1)\lambda\Delta\rho_0 - \frac{1}{r}\left(k\sqrt{\mu g r}\cos\theta \mp \sin\theta\right)\rho_0^2 V'_e(\rho_0) \tag{25}$$

Based on the obtained δ_1 and δ_2, we can determine that the real and imaginary parts of δ_k are respectively:

$$\begin{cases} R_e(\delta_k) \approx \begin{pmatrix} \frac{1}{a}\left(\frac{k\sqrt{\mu g r}\cos\theta \mp \sin\theta}{2r}\rho_0 V'_e(\rho_0)\right)^2 \\ + \frac{k\sqrt{\mu g r}\cos\theta \mp \sin\theta}{4r}V'_e(\rho_0) \\ + \frac{k\sqrt{\mu g r}\cos\theta \mp \sin\theta}{4ar}(l+1)\lambda\Delta\rho_0 V'_e(\rho_0) \end{pmatrix} k^2 - O\left(k^4\right) \\ Im(\sigma_k) \approx -\left(\omega_0 r + \frac{k\sqrt{\mu g r}\cos\theta \mp \sin\theta}{2}\rho_0 V'_e(\rho_0)\right)k + O\left(k^3\right) \end{cases} \tag{26}$$

The critical propagation velocity $c(\rho_0) = \omega_0 r + \frac{k\sqrt{\mu g r}\cos\theta \mp \sin\theta}{2}\rho_0 V'_e(\rho_0)$.

KdV-Burgers equation

In order to understand the formation and propagation characteristics of density waves near the neutral stability curve, we perform the nonlinear stability analysis on the proposed continuum model when the above stability condition Eq (25) is not satisfied. For a start, we introduce the following new coordinate transformation to the new model:

$$z = \varphi - ct \tag{27}$$

where c is the critical propagation velocity given above, φ and t are corresponding position variables and time variables. By rearranging the above transformation, we have $\varphi = z + ct$ and $t = \frac{\varphi - z}{c}$, respectively.

Incorporating Eq (27) into Eq (16), we get:

$$\begin{cases} -c\rho_z + q_z = 0 \\ -c\omega_z + \omega\omega_z = a\left(\frac{k\sqrt{\mu g r}\cos\theta \mp \sin\theta}{2r}V_e(\rho) - \omega\right) + \frac{(l+1)(2l+1)}{12}\lambda\omega_{zz}\Delta^2 \\ + \frac{l+1}{2}\lambda\Delta\omega_z + a\frac{k\sqrt{\mu g r}\cos\theta \mp \sin\theta}{2r}V'_e(\rho)\left(\frac{\rho_z}{2\rho} + \frac{\rho_{zz}}{6\rho^2}\right) \end{cases} \tag{28}$$

where $q = \rho \times \omega r$, and the first- and second- derivative of ω to z are:

$$\omega_z = \frac{1}{r}\left(\frac{c\rho_z}{\rho} - \frac{q\rho_z}{\rho^2}\right) \tag{29}$$

$$\omega_{zz}=\frac{1}{r}\left(\frac{c\rho_{zz}}{\rho}-\frac{2c\rho_z^2}{\rho^2}-\frac{q\rho_{zz}}{\rho^2}+\frac{2q\rho_z^2}{\rho^3}\right) \tag{30}$$

After performing Taylor expansion of q at steady state, then we have:

$$q=\rho\frac{k\sqrt{\mu gr\cos\theta}\mp\sin\theta}{2}V_e(\rho)+b_1\rho_z+b_2\rho_{zz} \tag{31}$$

Substituting Eq (29)–(31) into Eq (28), then we have:

$$\begin{aligned}&-\frac{c}{r}\left(\frac{c\rho_z}{\rho}-\frac{q\rho_z}{\rho^2}\right)+\frac{\omega}{r}\left(\frac{c\rho_z}{\rho}-\frac{q\rho_z}{\rho^2}\right)=a\left(\frac{k\sqrt{\mu gr\cos\theta}\mp\sin\theta}{2r}V_e(\rho)-\omega\right)\\&+\frac{(l+1)(2l+1)}{12r}\lambda\Delta^2\left(\frac{c\rho_{zz}}{\rho}-\frac{2c\rho_z^2}{\rho^2}-\frac{q\rho_{zz}}{\rho^2}+\frac{2q\rho_z^2}{\rho^3}\right)\\&+\frac{l+1}{2r}\lambda\Delta\left(\frac{c\rho_z}{\rho}-\frac{q\rho_z}{\rho^2}\right)+a\frac{k\sqrt{\mu gr\cos\theta}\mp\sin\theta}{2r}V'_e(\rho)\left(\frac{\rho_z}{2\rho}+\frac{\rho_{zz}}{6\rho^2}\right)\end{aligned} \tag{32}$$

Given that ρ_z and ρ_{zz} are not always zero, to guarantee that the above formula is established, the corresponding coefficients of ρ_z and ρ_{zz} in the above formula must always. be zero. After sorting, we have:

$$\begin{cases}b_1=\left(\frac{l+1}{2a}\lambda\Delta+\frac{c}{a}-\frac{k\sqrt{\mu gr\cos\theta}\mp\sin\theta}{2ar}V_e(\rho)\right)\\\quad\left(c-\frac{k\sqrt{\mu gr\cos\theta}\mp\sin\theta}{2}V_e(\rho)\right)+\frac{k\sqrt{\mu gr\cos\theta}\mp\sin\theta}{4}V'_e(\rho)\\b_2=\frac{(l+1)(2l+1)}{12a}\lambda\Delta^2\left(c-\frac{k\sqrt{\mu gr\cos\theta}\mp\sin\theta}{2}V_e(\rho)\right)\\\quad+\frac{k\sqrt{\mu gr\cos\theta}\mp\sin\theta}{12\rho}V'_e(\rho)\end{cases} \tag{33}$$

Given that density ρ equals the sum of steady-state density ρ_0 and the corresponding disturbance term $\hat{\rho}(x,t)$, i.e., $\rho=\rho_0+\hat{\rho}(x,t)$, the item $\rho\frac{k\sqrt{\mu gr\cos\theta}\mp\sin\theta}{2}V_e(\rho)$ can be approximated as follows using Taylor expansion:

$$\begin{aligned}&\rho\frac{k\sqrt{\mu gr\cos\theta}\mp\sin\theta}{2}V_e(\rho)\approx\rho_0\frac{k\sqrt{\mu gr\cos\theta}\mp\sin\theta}{2}V_e(\rho_0)\\&\left(\rho\frac{k\sqrt{\mu gr\cos\theta}\mp\sin\theta}{2}V_e(\rho)\right)_\rho\Bigg|_{\rho=\rho_0}\hat{\rho}\\&+\frac{1}{2}\left(\rho\frac{k\sqrt{\mu gr\cos\theta}\mp\sin\theta}{2}V_e(\rho)\right)_{\rho\rho}\Bigg|_{\rho=\rho_0}\hat{\rho}^2\end{aligned} \tag{34}$$

Combining Eq (34) with Eq (31), and bringing it into Eq (28), then we have:

$$\begin{aligned}&-c\rho_z+\left(\rho\frac{k\sqrt{\mu gr\cos\theta}\mp\sin\theta}{2}V_e(\rho)\right)_\rho\rho_z+\\&\left(\rho\frac{k\sqrt{\mu gr\cos\theta}\mp\sin\theta}{2}V_e(\rho)\right)_{\rho\rho}\rho\rho_z+b_1\rho_{zz}+b_2\rho_{zzz}=0\end{aligned} \tag{35}$$

To obtain the standard KdV-Burgers equation corresponding to Eq (35), the following coordinate transformation is introduced:

$$U=-\left[\left(\rho\frac{k\sqrt{\mu gr\cos\theta}\mp\sin\theta}{2}V_e(\rho)\right)_\rho+\left(\rho\frac{k\sqrt{\mu gr\cos\theta}\mp\sin\theta}{2}V_e(\rho)\right)_{\rho\rho}\rho\right],$$
$$X=mx,\quad T=-mt \tag{36}$$

Applying Eq (36) to Eq (35), then the following standard KdV-Burgers equation is derived:

$$U_T+UU_X-mb_1U_{XX}-m^2b_2U_{XXX}=0 \tag{37}$$

Based on the conclusions of the literature[61,62], we can obtain one of the solutions as:

$$U=-\frac{3(-mb_1)^2}{25(-m^2b_2)}\left[\begin{aligned}&1+2\tanh\left(\pm\frac{-mb_1}{10m^2}\right)\times\left(X+\frac{6(-mb_1)^2}{25(-m^2b_2)}T+\zeta_0\right)\\&+\tanh^2\left(\pm\frac{-mb_1}{10m^2}\right)\times\left(X+\frac{6(-mb_1)^2}{25(-m^2b_2)}T+\zeta_0\right)\end{aligned}\right] \tag{38}$$

where ζ_0 is an arbitrary constant.

Numerical example

In this part, we will carry out a numerical simulation to verify the above theoretical analysis conclusions. Since the continuum model is a partial differential form and difficult to simulate, to facilitate follow-up analysis, we first discretized the proposed continuum model Eq (16) based on the finite difference method, and the discretization form of continuous equation corresponding to Eq (16) is:

$$\rho_i^{j+1}=\rho_i^j+\frac{\Delta t}{\Delta\varphi}\omega_i^j\left(\rho_{i-1}^j-\rho_i^j\right)+\frac{\Delta t}{\Delta\varphi}\rho_i^j\left(\omega_i^j-\omega_{i+1}^j\right) \tag{39}$$

1) if $\omega_i^j<c_i^j$, we adopt the forward difference format to the evolution equation of Eq (16), which is:

$$\begin{aligned}&\omega_i^{j+1}=\omega_i^j+\frac{\Delta t}{\Delta\varphi}\left(\omega_i^j-c_i^j\right)\left(\omega_{i+1}^j-\omega_i^j\right)+a\Delta t\left(\frac{k\sqrt{\mu gr\cos\theta}\mp\sin\theta}{2r}V_e\left(\rho_i^j\right)-\omega_i^j\right)\\&+\frac{(l+1)(2l+1)}{12\left(\rho_i^j\right)^2}\lambda\Delta t\frac{\left(\omega_{i+1}^j-2\omega_i^j+\omega_{i-1}^j\right)}{(\Delta\varphi)^2}\\&+a\Delta t\frac{k\sqrt{\mu gr\cos\theta}\mp\sin\theta}{2r}V'_e\left(\rho_i^j\right)\left(\frac{\rho_i^j-\rho_{i-1}^j}{2(\Delta\varphi)\rho_i^j}+\frac{\rho_{i+1}^j-2\rho_i^j+\rho_{i-1}^j}{6\left(\rho_i^j\right)^2(\Delta\varphi)^2}\right)\end{aligned} \tag{40}$$

2) if $\omega_i^j\geqslant c_i^j$, we adopt the backward difference format to the evolution equation of Eq (16), i.e.,

$$\begin{aligned}&\omega_i^{j+1}=\omega_i^j+\frac{\Delta t}{\Delta\varphi}\left(\omega_i^j-c_i^j\right)\left(\omega_i^j-\omega_{i-1}^j\right)+\\&a\Delta t\left(\frac{k\sqrt{\mu gr\cos\theta}\mp\sin\theta}{2r}V_e\left(\rho_i^j\right)-\omega_i^j\right)\\&+\frac{(l+1)(2l+1)}{12\left(\rho_i^j\right)^2}\lambda\Delta t\frac{\left(\omega_{i+1}^j-2\omega_i^j+\omega_{i-1}^j\right)}{(\Delta\varphi)^2}\\&+a\Delta t\frac{k\sqrt{\mu gr\cos\theta}\mp\sin\theta}{2r}V'_e\left(\rho_i^j\right)\left(\frac{\rho_i^j-\rho_{i-1}^j}{2(\Delta\varphi)\rho_i^j}+\frac{\rho_{i+1}^j-2\rho_i^j+\rho_{i-1}^j}{6\left(\rho_i^j\right)^2(\Delta\varphi)^2}\right)\end{aligned} \tag{41}$$

where $c_i^j=\frac{l+1}{2\rho_i^j}\lambda$, ρ_i^j and ω_i^j represent the instantaneous density and velocity information of position i at time j, respectively; Δt and $\Delta\varphi$ are time and space steps, respectively.

Shock waves and rarefaction waves

Shock waves and rarefaction waves are not uncommon in the real traffic environment. When vehicles merge from the on-ramp into the main road, the density of the main road will increase significantly, where the fluctuation is called the shock wave. Alternately, if vehicles leave the main road from the exit ramp, the density of the main road steepness will drop, where the fluctuation is called the rarefaction wave. To verify whether the new model can simulate common traffic conditions well, as a start, we apply Riemann initial conditions[63] to the proposed continuum model to simulate shock waves and rarefaction wave phenomena in real traffic scenarios. The two Riemann initial conditions are:

$$(i)\,\rho_u^1 = 0.04, \quad \rho_d^1 = 0.18 \tag{42}$$

$$(ii)\,\rho_u^2 = 0.18, \quad \rho_d^2 = 0.04 \tag{43}$$

where ρ_u and ρ_d represent the density information of upstream and downstream roads, respectively, conditions (i) and (ii) are often used to simulate shock waves and rarefaction waves, respectively; and the initial velocities corresponding to different conditions are given by:

$$\rho_u^{1,2} = V_e\left(\rho_u^{1,2}\right), \rho_d^{1,2} = V_e\left(\rho_d^{1,2}\right) \tag{44}$$

Similar to the literature[64], the following speed-density relationship is adopted:

$$V_e(\rho) = v_f\left[1 - \exp\left(1 - \exp\left(\frac{c_m}{v_f}\left(\frac{\rho_m}{\rho} - 1\right)\right)\right)\right] \tag{45}$$

Table 3. Parameter settings corresponding to Case I.

Parameter	Value	Unit
v_f	30	m/s
L	20	km
c_m	11	–
ρ_m	0.2	veh/m
a	0.3	s^{-1}
λ	0.3	–
k	0.1	–
g	9.8	m/s^2
r	60	m
l	3	–
Δt	1	s
Δx	100	m

where v_f represents the free flow velocity; ρ_m represents the maximum density; and c_m represents the kinetic velocity under the blocking density. The specific values of default parameters are listed in Table 3.

As shown in Figs 3 & 4, the proposed continuum model can replicate shock waves and rarefaction waves for both uphill and downhill scenes. Compared to the uphill scenario, the density waves are smoother for the downhill scenario. This result is consistent with the subsequent conclusions.

Local cluster effect

Next, we will analyze the local cluster effect of the proposed continuum model to explore the evolution of initial disturbances. In doing so, we adopt the boundary conditions given by Herrmann & Kerner[65] to initialize the model density:

$$\rho(\varphi,0) = \rho_0 + \Delta\rho_0\left\{\cosh^{-2}\left[\frac{160}{L}\left(\varphi - \frac{5L}{16}\right)\right] - \frac{1}{4}\cosh^{-2}\left[\frac{40}{L}\left(\varphi - \frac{11L}{32}\right)\right]\right\} \tag{46}$$

where L represents the length of the road; ρ_0 represents the initial density, and $\Delta\rho_0$ is the initial disturbance of density. To simulate the iterative process of density waves, we adopt the following periodic boundary conditions:

$$\rho(L,t) = \rho(0,t), \quad v(L,t) = v(0,t) \tag{47}$$

The relationship of the average speed and density can be found in the literature[66]. The values of default parameters have been specified in Table 4.

$$V_e(\rho) = v_f\left[\left(1 + \exp\frac{\rho/\rho_m - 0.25}{0.06}\right)^{-1} - 3.72\times10^{-6}\right]. \tag{48}$$

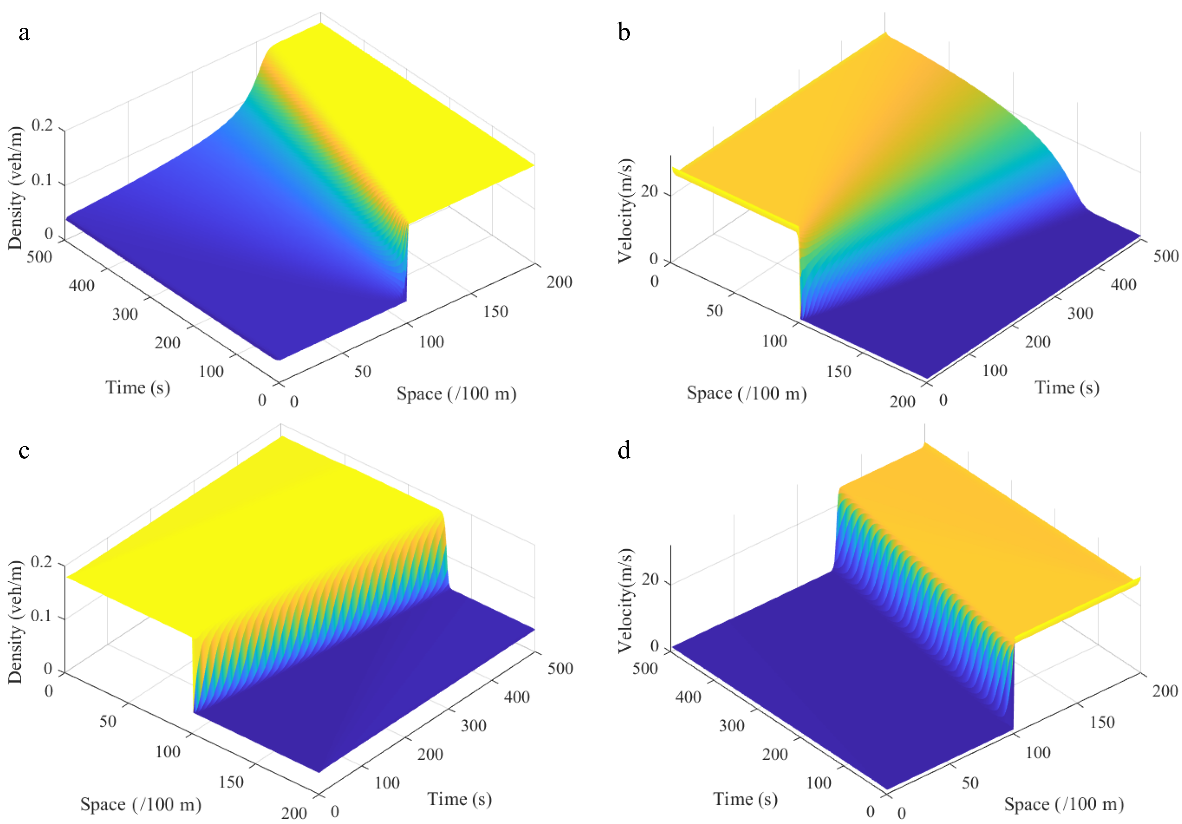

Fig. 3 Shock waves under the Riemann initial condition (i), where: (a) density $\rho(\varphi,t)$; (b) velocity ωr; the rarefaction waves under the Riemann initial condition (ii), where: (c) density $\rho(\varphi,t)$; (d) velocity ωr. (Under downhill scenes) ($\theta = = -6$).

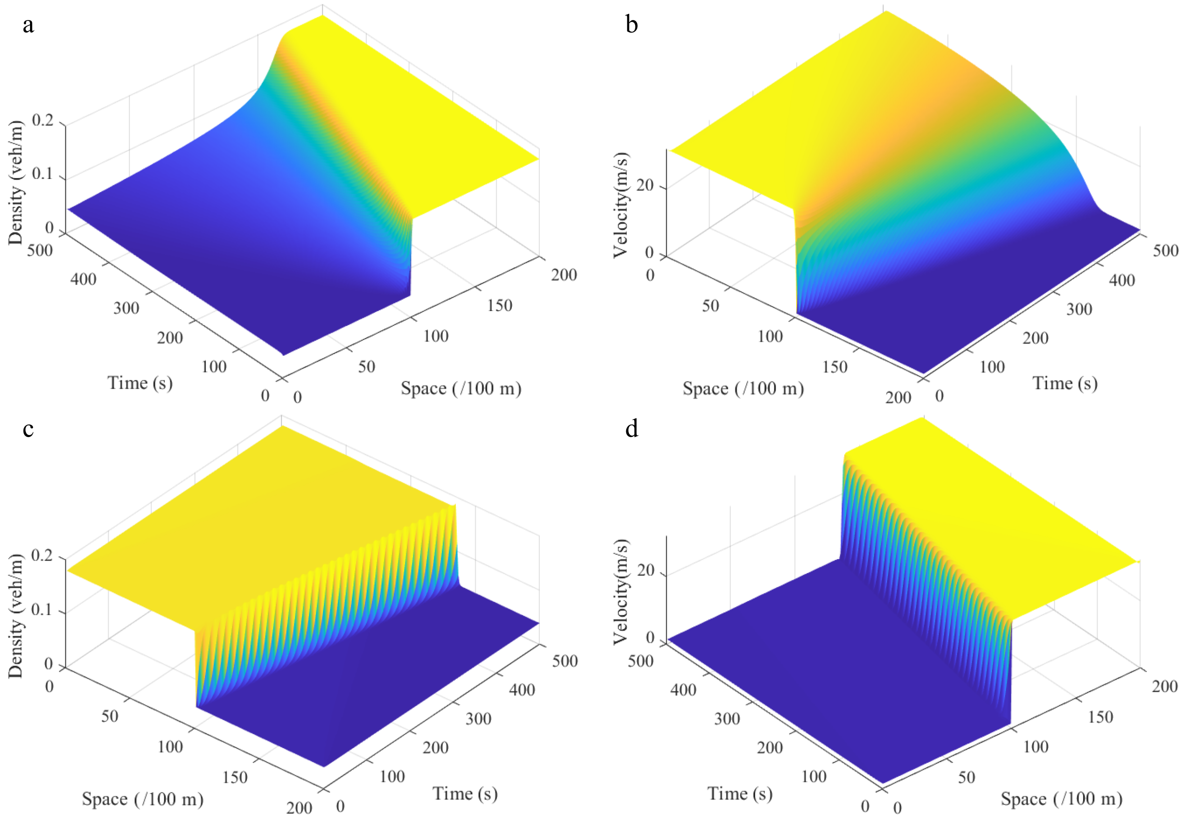

Fig. 4 Shock waves under the Riemann initial condition (i), where: (a) density $\rho(\varphi,t)$; (b) velocity ωr; the rarefaction waves under the Riemann initial condition (ii), where: (c) density $\rho(\varphi,t)$; (d) velocity ωr. (Under uphill scenes) (θ = 6).

Table 4. Parameter settings.

Parameter	Value	Unit
v_f	30	m/s
L	32.2	km
ρ_m	0.2	veh/m
a	0.34	s^{-1}
λ	0.3	–
k	0.1	–
g	9.8	m/s^2
Δt	1	s
Δx	100	m

Figure 5 describes the spatiotemporal diagram of the density wave affected by the initial disturbance under different initial densities ρ_0. When ρ_0 = 0.042 veh/m, the density waves remain stable. When ρ_0 increases from 0.042 to 0.051 veh/m, the density fluctuation appears as shown in Fig. 5b. When ρ_0 = 0.065 veh/m, the stop-and-go waves appear in Fig. 5c, and the characteristics can be described by the density waves by solving the KdV-Burgers equation in the nonlinear stability analysis. Finally, when ρ_0 = 0.079 veh/m, the initial disturbance disappears in Fig. 5d and eventually the density wave returns to the steady state. Typically, when ρ_0 exceeds 0.079 veh/m, the density fluctuations phenomenon will never appear. Therefore, the traffic flow is unstable once the initial density belongs to the interval [0.042 veh/m, 0.079 veh/m].

Figure 6 describes the spatiotemporal diagram of density waves affected by the initial disturbance under different slope angles θ. $\theta > 0$ and $\theta < 0$ correspond to the uphill scenario and downhill scenario, respectively. For the downhill scenario, the fluctuation amplitude of the density wave is the smallest when θ= −10. As the absolute value of the parameter θ gradually decreases, the density fluctuation gradually aggravates. For the uphill scenario, the effect of parameter θ is the opposite. Specifically, the fluctuation amplitude increases with the increase of the parameter θ. The instantaneous density distribution of road traffic flow as shown in Fig. 7 at t = 3,000 s reinforces the conclusion of Fig. 6.

To analyze the influence of the radius of curvature r in the gyroidal road on the stability of traffic flow, we compare the evolution of the initial disturbance over time corresponding to different curvature radius r under a downhill scenario, and the results are shown in Fig. 8. The parameters are set as ρ_0, θ = −6, l = 2. As the parameter r increases, the fluctuation amplitude of the initial disturbance decreases. This indicates that a larger radius of curvature r on gyroidal roads will worsen traffic flow stability. Figure 9 shows the instantaneous density distribution corresponding to Fig. 8 at t = 3,000 s. The evolution of the initial disturbance over time in Fig. 9a is gradually diluted, and finally, the traffic returns to the equilibrium state without any density fluctuation amplitude. As the parameter r increases, the density fluctuation amplitude gradually expands, of which results are consistent with that of Fig. 8. Moreover, Figs 10 & 11 show the evolution of initial disturbance over time corresponding to different curvature radius r under an uphill scenario. As the curvature r increases, the fluctuation amplitude and frequency of road density waves become more severe, which is equivalent to the uphill scenario (Figs 8 & 9).

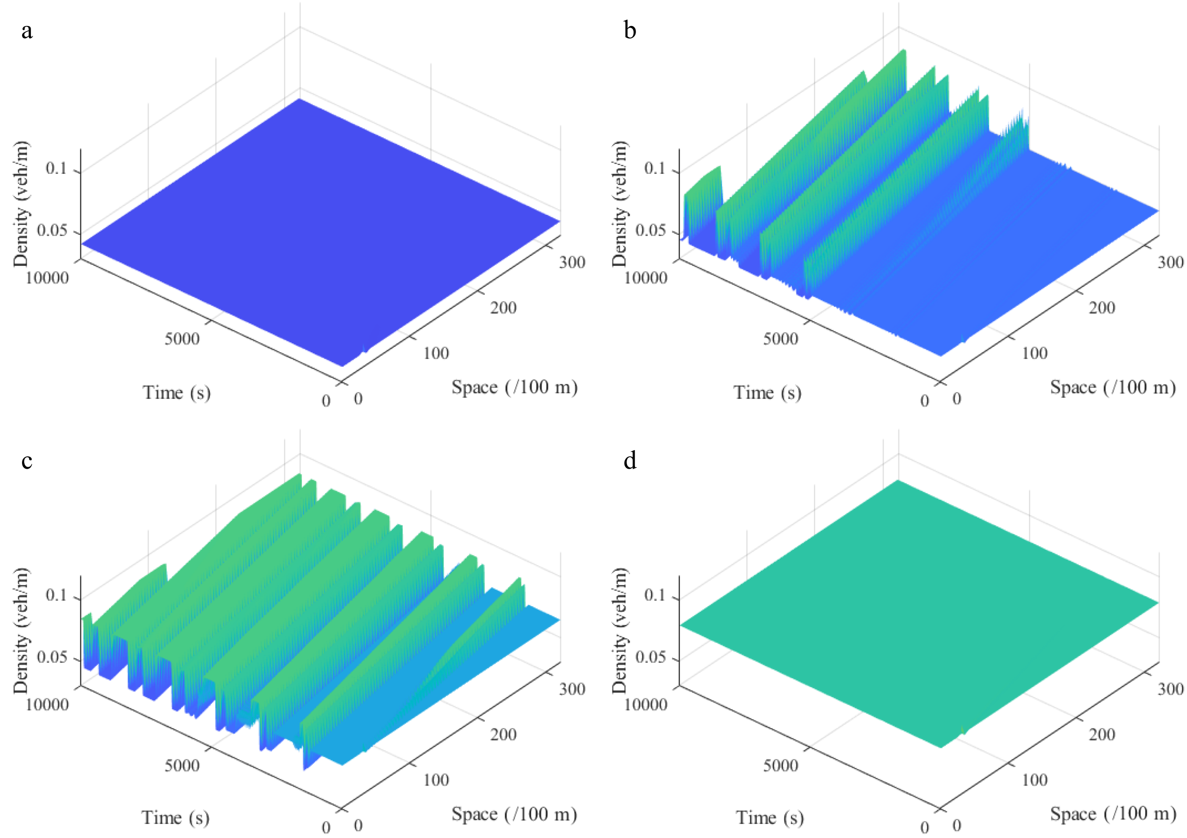

Fig. 5 Spatiotemporal diagram of density waves affected by the initial disturbance under different initial densities ρ_0, where: (a) $\rho_0 = 0.042$ veh/m; (b) $\rho_0 = 0.051$ veh/m; (c) $\rho_0 = 0.065$ veh/m; (d) $\rho_0 = 0.079$ veh/m. ($l = 2$, $\theta = 0$, $r = 75$).

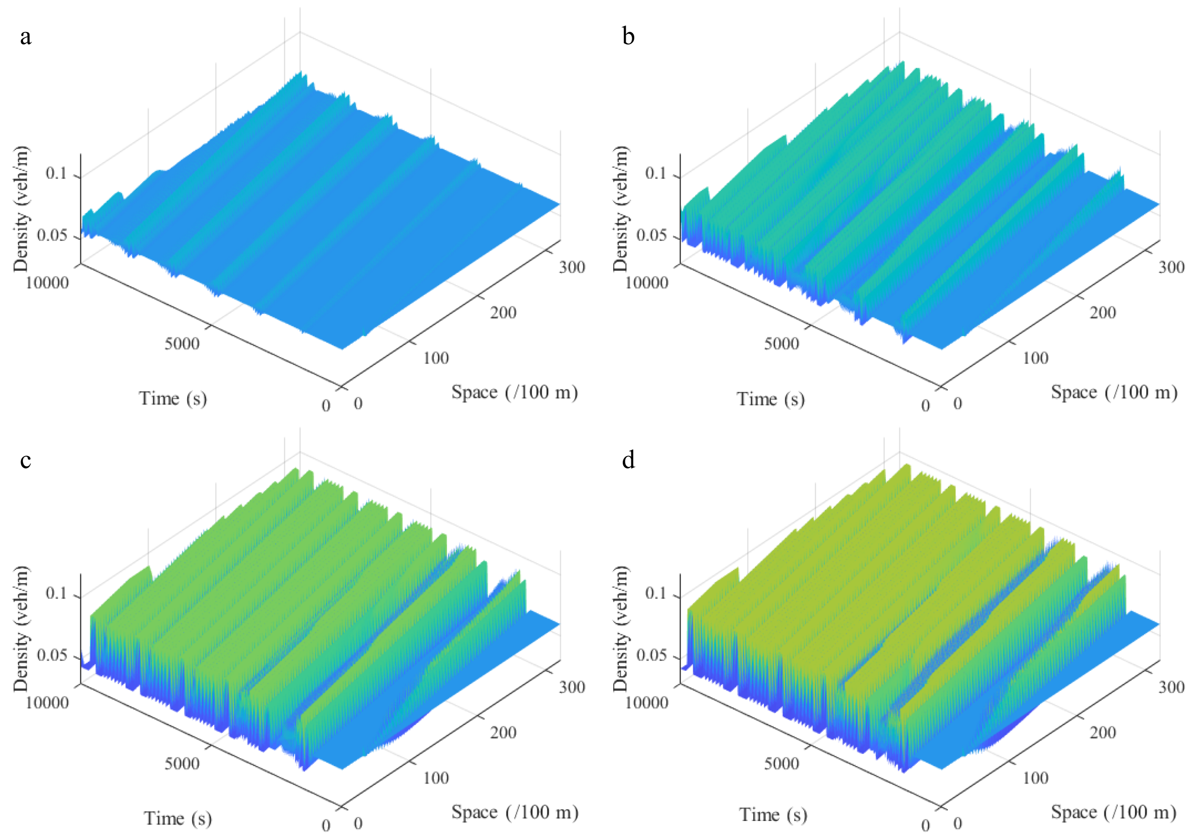

Fig. 6 Spatiotemporal diagram of density waves affected by the initial disturbance under different slope angles θ, where: (a) $\theta = -10$; (b) $\theta = -5$; (c) $\theta = 5$; (d) $\theta = 10$. ($l = 2$, $\rho_0 = 0.06$, $r = 75$).

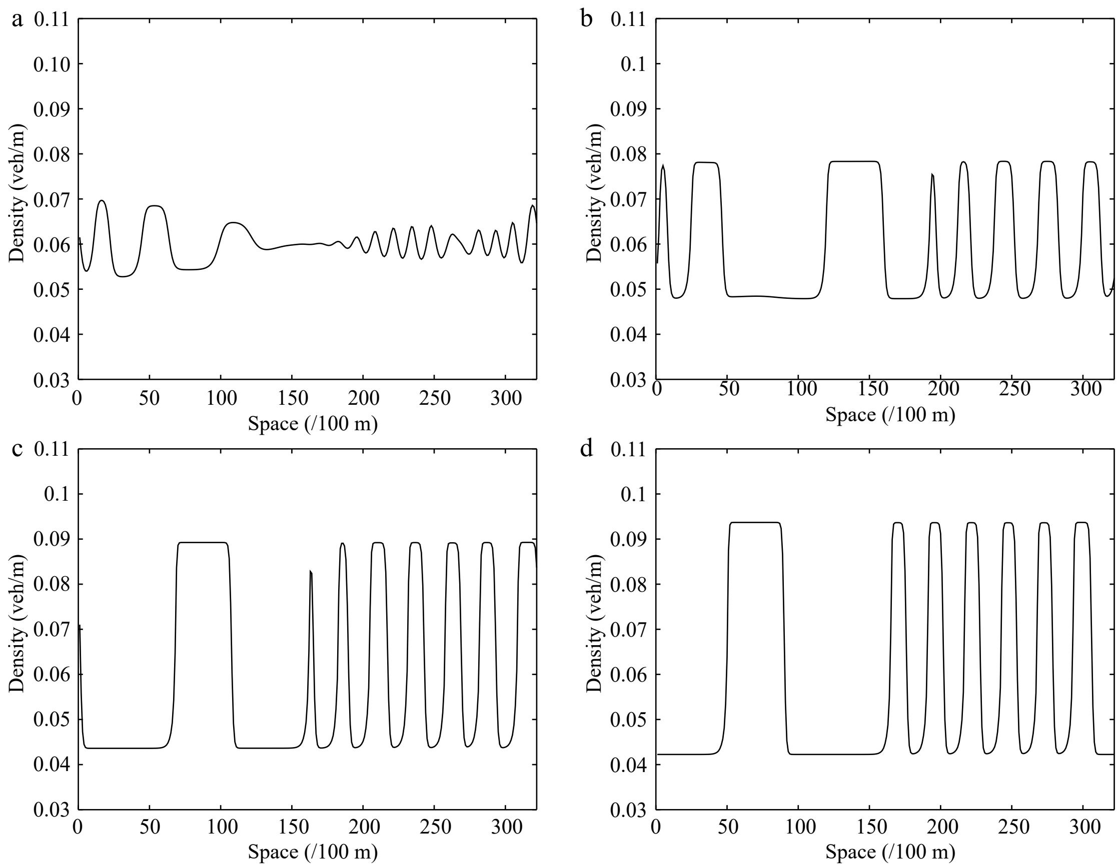

Fig. 7 Instantaneous density distribution of traffic flow corresponding to Fig. 6 at $t = 3{,}000$ s.

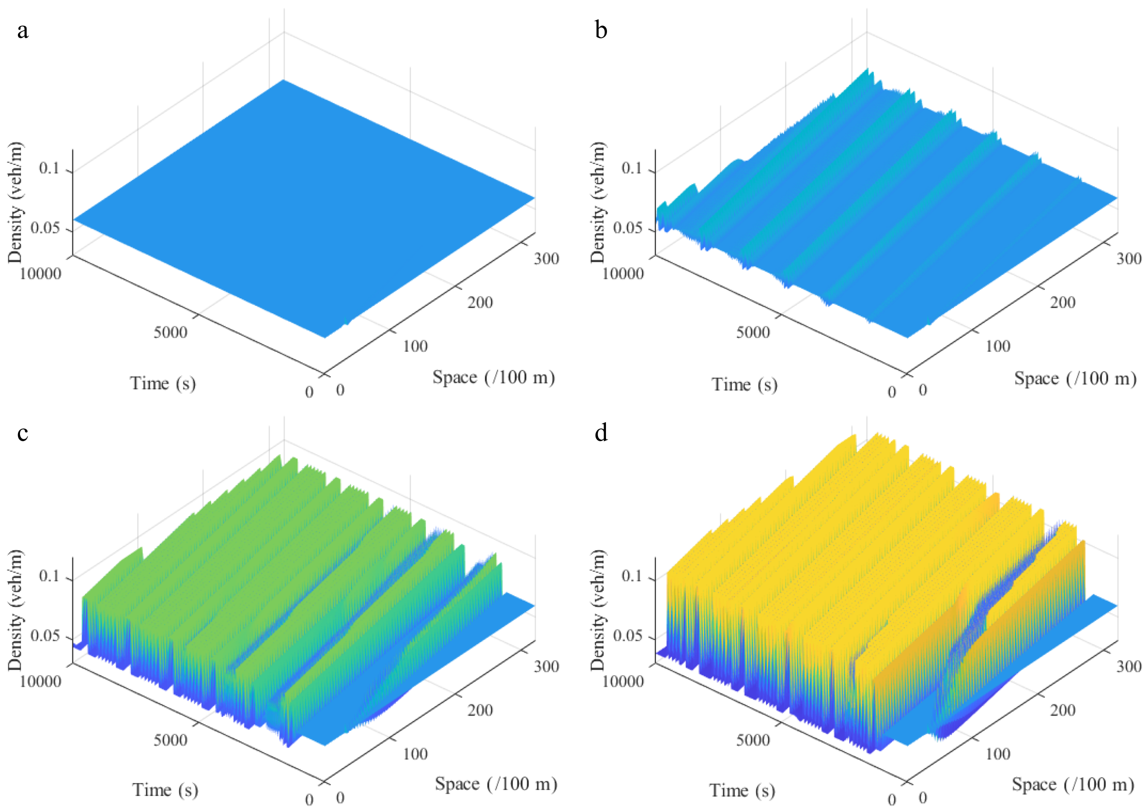

Fig. 8 Spatiotemporal diagram of density waves affected by the initial disturbance corresponding to different curvature radiuses r under the downhill scenario, where: (a) $r = 50$; (b) $r = 70$; (c) $r = 90$; (d) $r = 120$. ($\rho_0 = 0.06$, $\theta = -6$, $l = 2$).

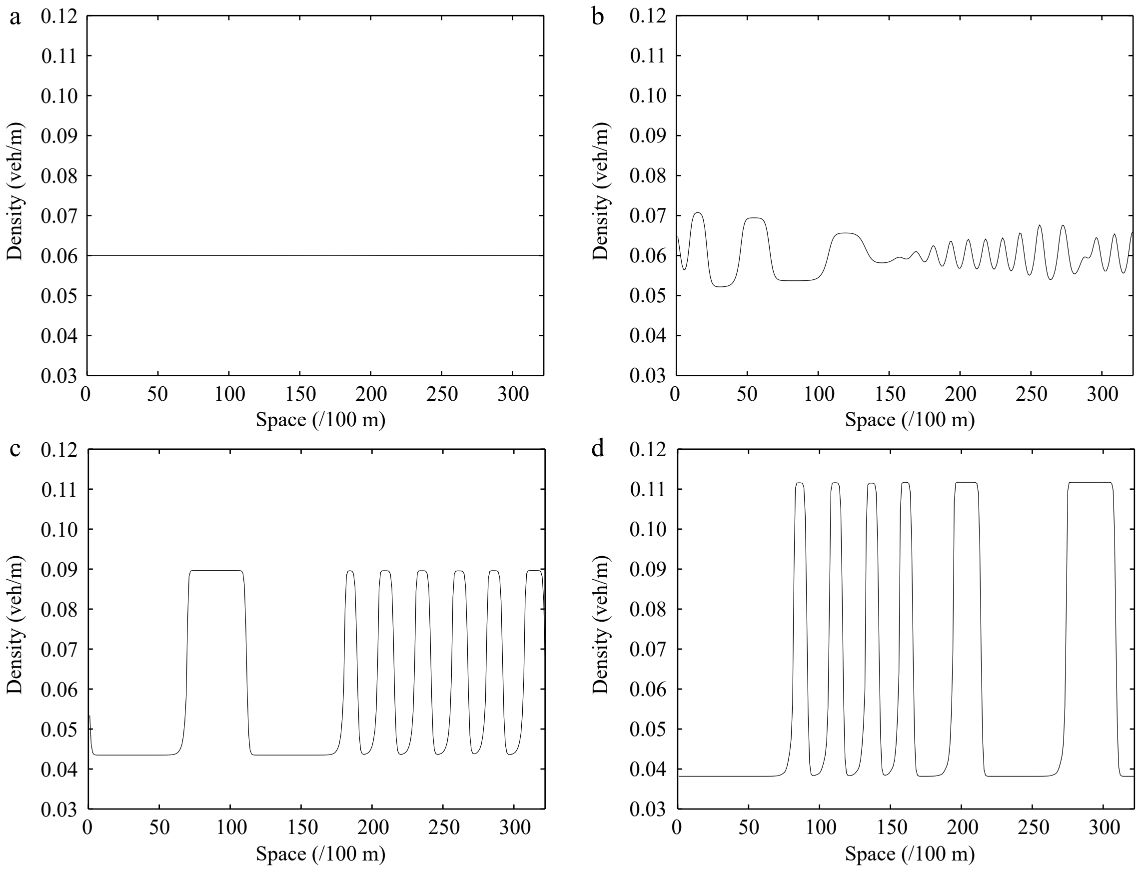

Fig. 9 Instantaneous density distribution of road traffic flow corresponding to Fig. 8 at $t = 3{,}000$ s.

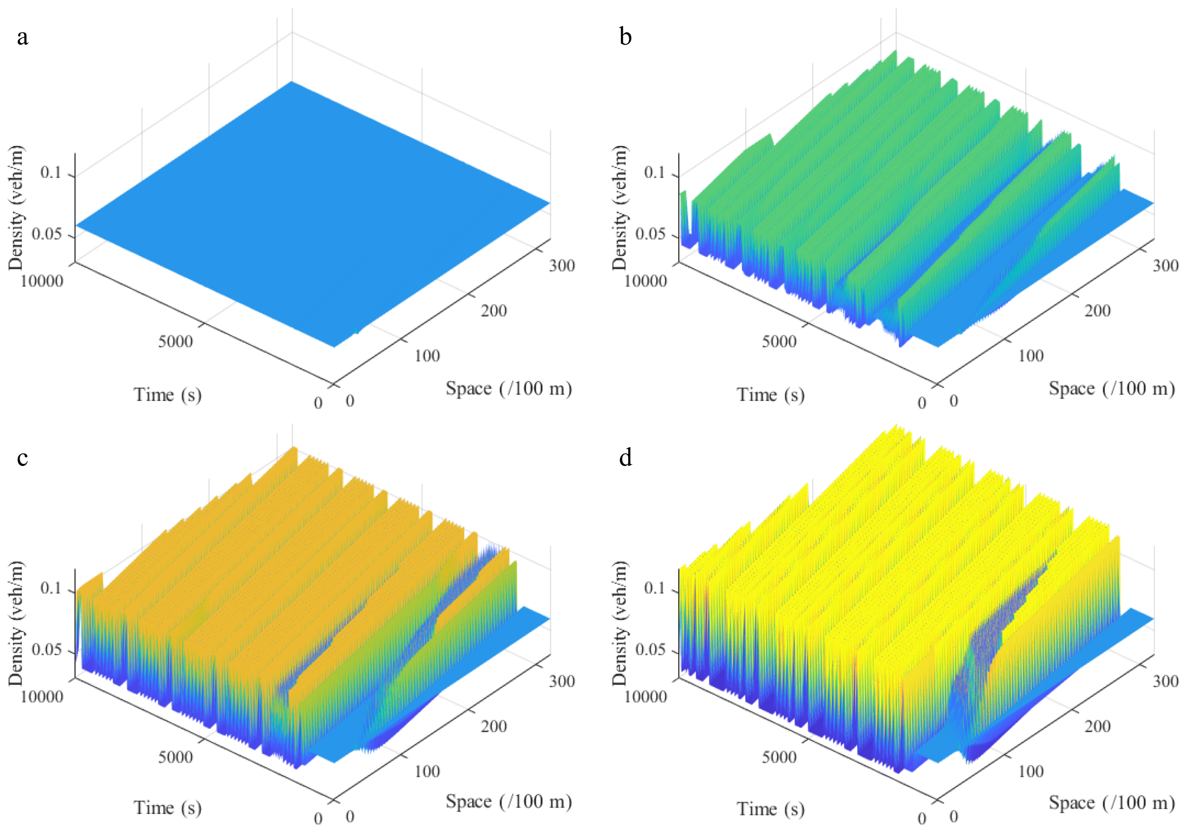

Fig. 10 Spatiotemporal diagram of density waves affected by the initial disturbance corresponding to different curvature radiuses r under the uphill scenario, where: (a) $r = 50$; (b) $r = 70$; (c) $r = 90$; (d) $r = 120$. ($\rho_0 = 0.06$, $\theta = 6$, $l = 2$).

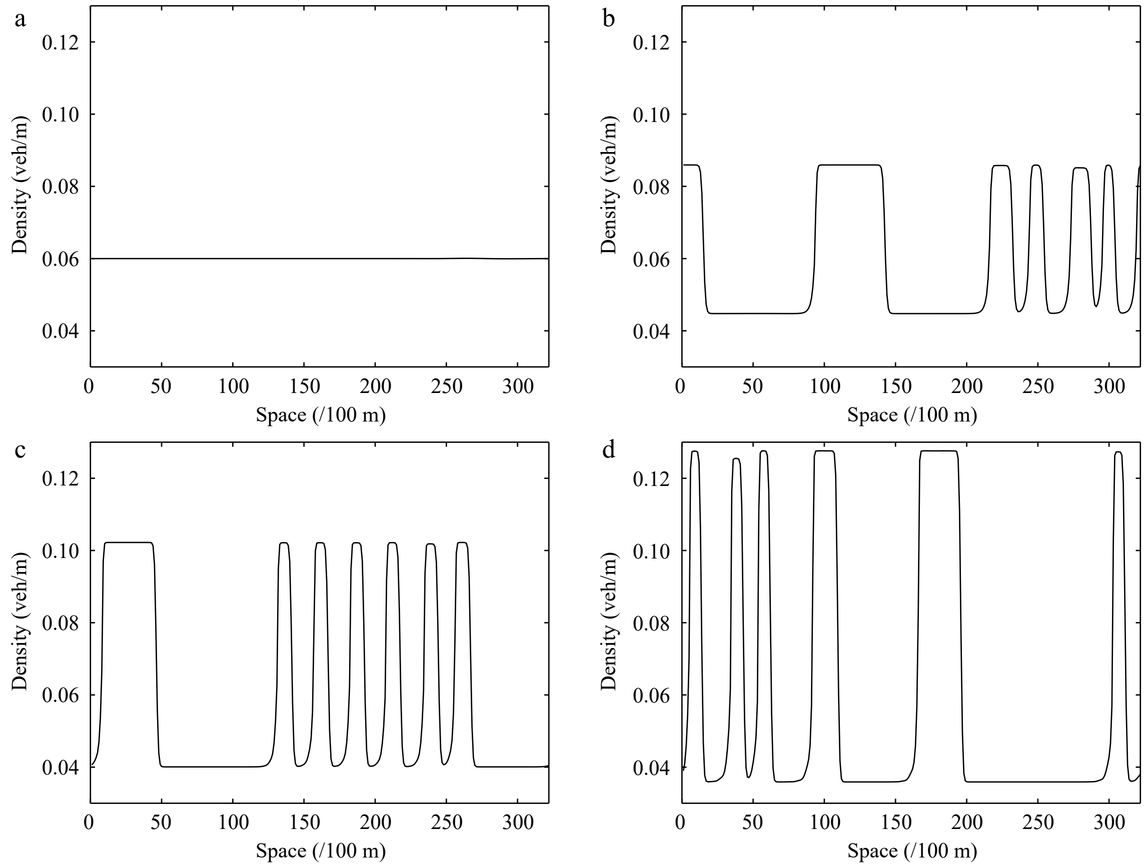

Fig. 11 Instantaneous density distribution of road traffic flow corresponding to Fig. 10 at $t = 3{,}000$ s.

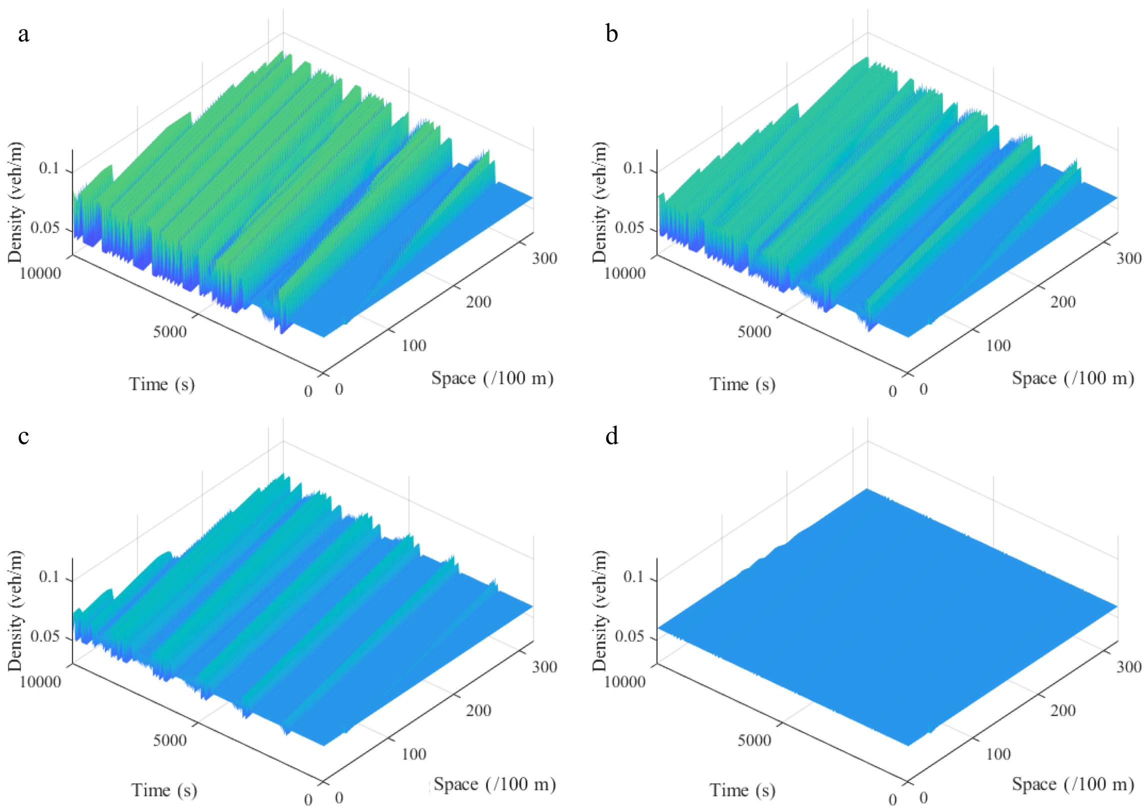

Fig. 12 Spatiotemporal diagram of density waves affected by the initial disturbance corresponding to different values of parameter l under a downhill scenario, where: (a) $l = 0$; (b) $l = 1$; (c) $l = 2$; (d) $l = 3$. ($\rho_0 = 0.06$, $\theta = -8$, $r = 75$).

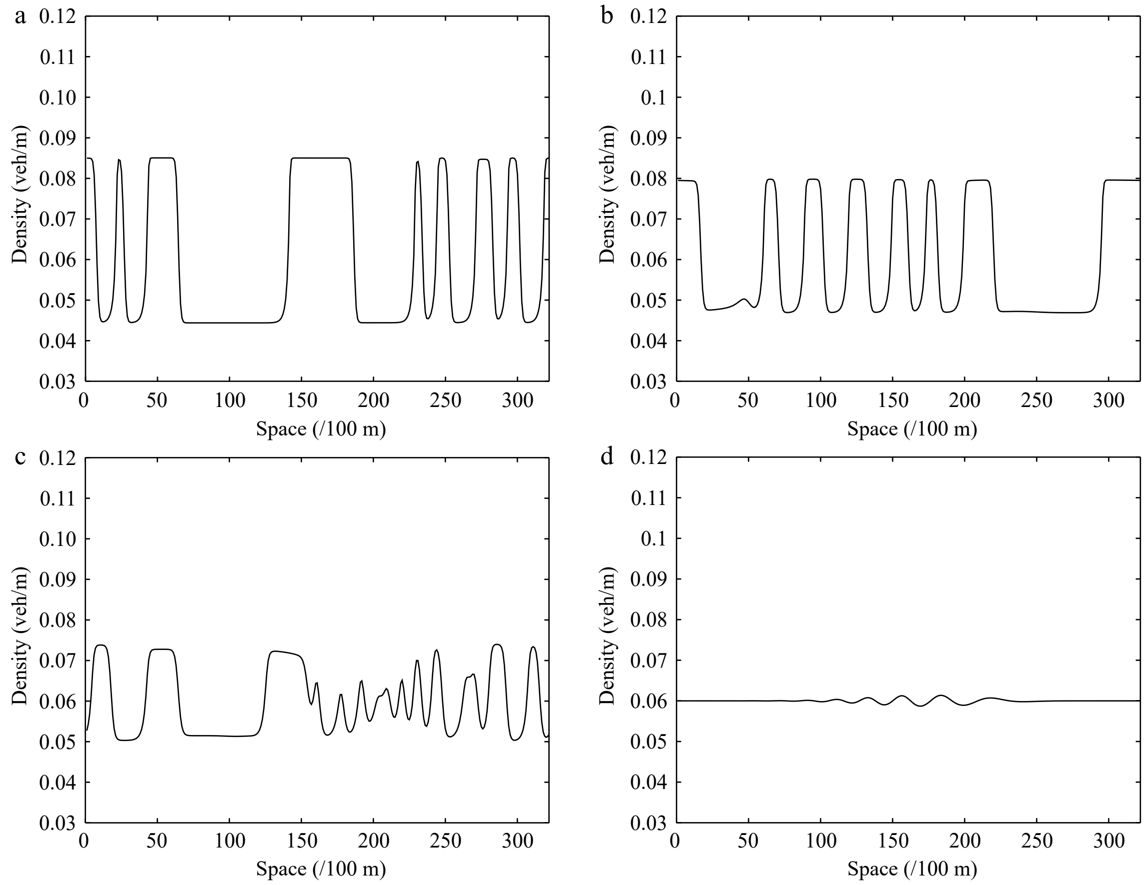

Fig. 13 Instantaneous density distribution of traffic flow corresponding to Fig. 12 at $t = 3{,}000$ s.

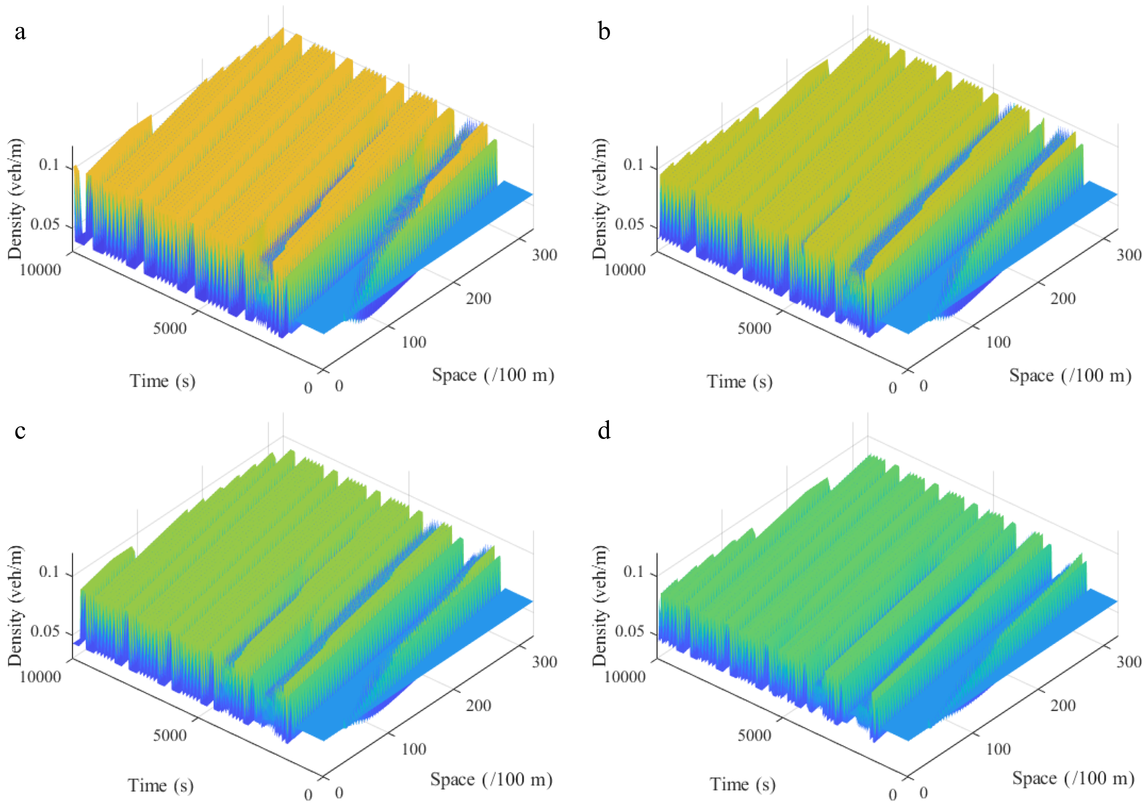

Fig. 14 Spatiotemporal diagram of density waves affected by the initial disturbance corresponding to different values of parameter l under the uphill scenario, where: (a) $l = 0$; (b) $l = 1$; (c) $l = 2$; (d) $l = 3$. ($\rho_0 = 0.06$, $\theta = 8$, $r = 75$).

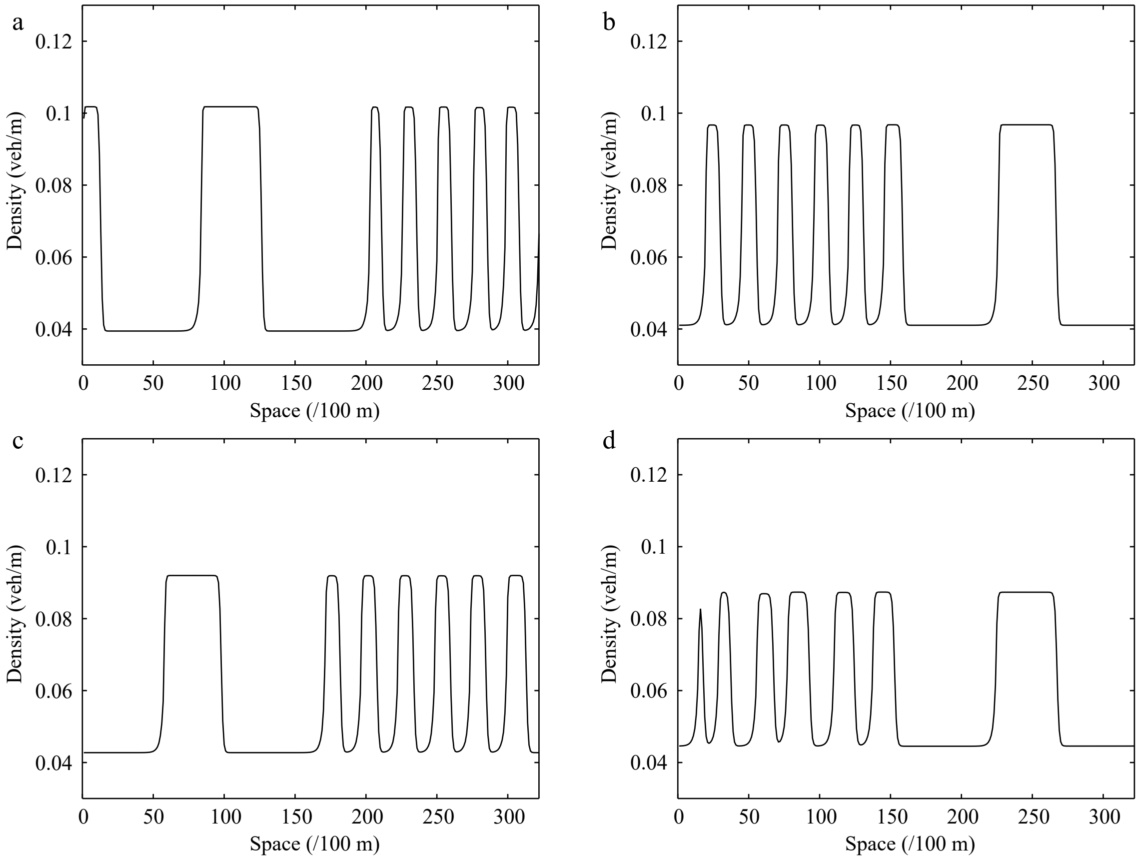

Fig. 15 Instantaneous density distribution of traffic flow corresponding to Fig. 14 at t = 3,000 s.

Figures 12–15 describe the spatiotemporal diagram of density waves affected by the initial disturbance under different values of the parameter l, where Figs 12 & 13 and Figs 14 & 15 correspond to the downhill and uphill scenarios, respectively. When $l = 0$, the model does not have new items. As the parameter l increases, the density wave is gradually smoothed, which implies that the new items are beneficial to improve the robustness of traffic flow when $l > 0$. Specifically, the larger the parameter l, the more conducive to suppressing traffic congestion, which verifies the benefits of a connected vehicle environment.

Concluding remarks

To pave the way for effectively controlling the system in a future connected vehicle environment, we propose a new continuous model taking into account the effect of the average velocity of multiple vehicles ahead on gyroidal roads. In linear and nonlinear stability analysis, the neutral stability curve and KdV-Burger equation corresponding to the model are obtained *via* the perturbation method. Solving the above KdV-Burger equation yields the density wave solution that can depict the propagation and evolution characteristics of traffic jams near the critical point. Finally, we carried out some numerical simulations to verify the theoretical analysis conclusions. Key findings and their implications are summarized as follows:

(I) The proposed model can well reproduce the shock wave and rarefaction wave under the Riemann initial conditions;

(II) The local cluster effect of the proposed continuum model is analyzed to explore the evolution of initial disturbances. Results show that the number of vehicles ahead considered l, radius of curvature r, slope angle θ will directly affect the stability of traffic flow. Specifically, a higher value of parameter l contributes to suppressing the disturbance, which also explains the benefit of connected vehicles. As the parameter r or θ increases, traffic jams are more likely to take place.

In future research, more realistic factors can be embedded in the model framework, such as lane-changing, vehicle overtaking behavior, and heterogeneous vehicles. In addition, the simulation environment of this research is period bounded, that is, the merge of external vehicles and the leaving of vehicles in the platoon are not considered. Therefore, another line of future research may concern the open-ended simulation environment.

Acknowledgments

This work is jointly supported by Guangdong Basic and Applied Research Foundation (Project No. 2022A1515010948, 2019A1515111200, 2019A1515110837, 2023A1515011696), the National Science Foundation of China (Project No. 72071079, 52272310).

Conflict of interest

The authors declare that they have no conflict of interest. Wu Weitiao is the Editorial Board member of *Digital Transportation and Safety*. He was blinded from reviewing or making decisions on the manuscript. The article was subject to the journal's standard procedures, with peer-review handled independently of this Editorial Board member and his research groups.

Dates

Received 23 November 2022; Accepted 21 April 2023; Published online 29 June 2023

References

1. Huang L, Zhai C, Wang H, Zhang R, Qiu Z, et al. 2020. Cooperative Adaptive Cruise Control and exhaust emission evaluation under heterogeneous connected vehicle network environment in urban city. *Journal of Environmental Management* 256:109975
2. Zhai C, Wu W. 2021. Self-delayed feedback car-following control with the velocity uncertainty of preceding vehicles on gradient roads. *Nonlinear Dynamics* 106:3379−400
3. Zhai C, Wu W. 2018. A new car-following model considering driver' s characteristics and traffic jerk. *Nonlinear Dynamics* 93:2185−99
4. Ma M, Ma G, Liang S. 2021. Density waves in car-following model for autonomous vehicles with backward looking effect. *Applied Mathematical Modelling* 94:1−12
5. Ma G, Ma M, Liang S, Wang Y, Guo H. 2021. Nonlinear analysis of the car-following model considering headway changes with memory and backward looking effect. *Physica A: Statistical Mechanics and Its Applications* 562:125303
6. Ma G, Ma M, Liang S, Wang Y, Zhang Y. 2020. An improved car-following model accounting for the time-delayed velocity difference and backward looking effect. *Communications in Nonlinear Science and Numerical Simulation* 85:105221
7. Jiang Y, Wang S, Yao Z, Zhao B, Wang Y. 2021. A cellular automata model for mixed traffic flow considering the driving behavior of connected automated vehicle platoons. *Physica A:Statistical Mechanics and Its Applications* 582:126262
8. Chen B, Sun D, Zhou J, Wong W, Ding Z. 2020. A future intelligent traffic system with mixed autonomous vehicles and human-driven vehicles. *Information Sciences* 529:59−72
9. Zhai C, Wu W. 2021. Designing continuous delay feedback control for lattice hydrodynamic model under cyber-attacks and connected vehicle environment. *Communications in Nonlinear Science and Numerical Simulation* 95:105667
10. Redhu P, Gupta AK. 2015. Jamming transitions and the effect of interruption probability in a lattice traffic flow model with passing. *Physica A: Statistical Mechanics and Its Applications* 421:249−60
11. Kaur D, Sharma S. 2020. A new two-lane lattice model by considering predictive effect in traffic flow. *Physica A: Statistical Mechanics and Its Applications* 539:122913
12. Sharma S. 2015. Lattice hydrodynamic modeling of two-lane traffic flow with timid and aggressive driving behavior. *Physica A: Statistical Mechanics and Its Applications* 421:401−11
13. Kaur R, Sharma S. 2017. Analysis of driver's characteristics on a curved road in a lattice model. *Physica A: Statistical Mechanics and Its Applications* 471:59−67
14. Redhu P, Gupta AK. 2015. Delayed-feedback control in a Lattice hydrodynamic model. *Communications in Nonlinear Science and Numerical Simulation* 27:263−70
15. Kaur R, Sharma S. 2018. Analyses of lattice hydrodynamic model using delayed feedback control with passing. *Physica A:Statistical Mechanics and Its Applications* 510:446−55
16. Kaur R, Sharma S. 2018. Analyses of a heterogeneous lattice hydrodynamic model with low and high-sensitivity vehicles. *Physics Letters A* 382:1449−55
17. Helbing D. 1995. Improved fluid-dynamic model for vehicular traffic. *Physical Review E* 51:3164−69
18. Lighthill M, Whitham G. 1955. On kinematic waves I. Flood movement in long rivers. *Proceedings of the Royal Society of London Series A Mathematical and Physical Sciences* 229:281−316
19. Lighthill MJ, Whitham GB. 1955. On kinematic waves II. A theory of traffic flow on long crowded roads. *Proceedings of the Royal Society of London Series A Mathematical and Physical Sciences* 229:317−45
20. Richards PI. 1956. Shock waves on the highway. *Operations Research* 4:42−51
21. Payne H. 1971. Models of freeway traffic and control: mathematical models of public systems. *Simulation Council Proceeding Series* 1(1):51−61
22. Daganzo CF. 1995. Requiem for second-order fluid approximations of traffic flow. *Transportation Research Part B: Methodological* 29:277−86
23. Zhang HM. 2002. A non-equilibrium traffic model devoid of gas-like behavior. *Transportation Research Part B:Methodological* 36:275−90
24. Jiang R, Wu Q, Zhu Z. 2002. A new continuum model for traffic flow and numerical tests. *Transportation Research Part B:Methodological* 36:405−19
25. Wang Z, Zhu W. 2023. Effects of electronic throttle dynamics in non-equilibrium heterogeneous traffic flow without lane discipline. *Applied Mathematical Modelling* 116:673−94
26. Ren W, Cheng R, Ge H. 2021. Bifurcation analysis of a heterogeneous continuum traffic flow model. *Applied Mathematical Modelling* 94:369−87
27. Ren W, Cheng R, Ge H. 2021. Bifurcation analysis for a novel heterogeneous continuum model considering electronic throttle angle changes with memory. *Applied Mathematics and Computation* 401:126079
28. Sun L, Jafaripournimchahi A, Hu W. 2020. A forward-looking anticipative viscous high-order continuum model considering two leading vehicles for traffic flow through wireless V2X communication in autonomous and connected vehicle environment. *Physica A: Statistical Mechanics and Its Applications* 556:124589
29. Sun L, Jafaripournimchahi A, Kornhauser A, Hu W. 2020. A new higher-order viscous continuum traffic flow model considering driver memory in the era of autonomous and connected vehicles. *Physica A: Statistical Mechanics and Its Applications* 547:123829
30. Liu H, Cheng R, Zhu K, Ge H. 2016. The study for continuum model considering traffic jerk effect. *Nonlinear Dynamics* 83:57−64
31. Cheng R, Ge H, Wang J. 2018. The nonlinear analysis for a new continuum model considering anticipation and traffic jerk effect. *Applied Mathematics and Computation* 332:493−505
32. Lyu H, Cheng R, Ge H. 2022. Bifurcation analysis of an extended macro model considering time delay and anticipation effect. *Physica A: Statistical Mechanics and Its Applications* 585:126434
33. Jafaripournimchahi A, Cai Y, Wang H, Sun L, Yang B. 2022. Stability analysis of delayed-feedback control effect in the continuum traffic flow of autonomous vehicles without V2I communication. *Physica A: Statistical Mechanics and Its Applications* 605:127975
34. Liu Z, Cheng R, Ge H. 2019. Research on preceding vehicle's taillight effect and energy consumption in an extended macro traffic model. *Physica A: Statistical Mechanics and Its Applications* 525:304−14
35. Zhai C, Wu W. 2021. A continuous traffic flow model considering predictive headway variation and preceding vehicle's taillight effect. *Physica A: Statistical Mechanics and Its Applications* 584:126364
36. Jiao Y, Ge H, Cheng R. 2019. Nonlinear analysis for a modified continuum model considering electronic throttle (ET) and backward looking effect. *Physica A: Statistical Mechanics and Its Applications* 535:122362
37. Wang Z, Ge H, Cheng R. 2018. Nonlinear analysis for a modified continuum model considering driver's memory and backward looking effect. *Physica A: Statistical Mechanics and Its Applications* 508:18−27

38. Cheng R, Ge H, Wang J. 2017. An improved continuum model for traffic flow considering driver's memory during a period of time and numerical tests. *Physics Letters A* 381:2792−800
39. Zhai Q, Ge H, Cheng R. 2018. An extended continuum model considering optimal velocity change with memory and numerical tests. *Physica A: Statistical Mechanics and Its Applications* 490:774−85
40. Cheng R, Ge H, Sun F, Wang J. 2018. An extended macro model accounting for acceleration changes with memory and numerical tests. *Physica A: Statistical Mechanics and Its Applications* 506:270−83
41. Zhai C, Wu W. 2018. Analysis of drivers' characteristics on continuum model with traffic jerk effect. *Physics Letters A* 382:3381−92
42. Cheng R, Ge H, Wang J. 2017. An extended continuum model accounting for the driver's timid and aggressive attributions. *Physics Letters A* 381:1302−12
43. Zhai C, Wu W. 2022. A continuum model considering the uncertain velocity of preceding vehicles on gradient highways. *Physica A: Statistical Mechanics and Its Applications* 588:126561
44. Chen J, Shi Z, Hu Y, Yu L, Fang Y. 2013. An extended macroscopic model for traffic flow on a highway with slopes. *International Journal of Modern Physics C* 24:1350061
45. Liu Z, Ge H, Cheng R. 2018. KdV–Burgers equation in the modified continuum model considering the effect of friction and radius on a curved road. *Physica A: Statistical Mechanics and Its Applications* 503:1218−27
46. Xue Y, Zhang Y, Fan D, Zhang P, He H. 2019. An extended macroscopic model for traffic flow on curved road and its numerical simulation. *Nonlinear Dynamics* 95:3295−307
47. Guan X, Cheng R, Ge H. 2021. Bifurcation control of optimal velocity model through anticipated effect and response time-delay feedback methods. *Physica A: Statistical Mechanics and Its Applications* 574:125972
48. Cheng R, Ge H, Wang J. 2017. KdV–Burgers equation in a new continuum model based on full velocity difference model considering anticipation effect. *Physica A: Statistical Mechanics and Its Applications* 481:52−9
49. Ngoduy D. 2021. Noise-induced instability of a class of stochastic higher order continuum traffic models. *Transportation Research Part B: Methodological* 150:260−78
50. Bouadi M, Jia B, Jiang R, Li X, Gao Z. 2022. Stability analysis of stochastic second-order macroscopic continuum models and numerical simulations. *Transportation Research Part B: Methodological* 164:193−209
51. Wang Z, Ge H, Cheng R. 2020. An extended macro model accounting for the driver's timid and aggressive attributions and bounded rationality. *Physica A: Statistical Mechanics and Its Applications* 540:122988
52. Tang T, Huang H, Shang H. 2017. An extended macro traffic flow model accounting for the driver's bounded rationality and numerical tests. *Physica A: Statistical Mechanics and Its Applications* 468:322−33
53. Zhu W, Yu R. 2014. A new car-following model considering the related factors of a gyroidal road. *Physica A: Statistical Mechanics and Its Applications* 393:101−11
54. Zhai C, Wu W. 2019. Car-following model based delay feedback control method with the gyroidal road. *International Journal of Modern Physics C* 30:1950073
55. Bando M, Hasebe K, Nakayama A, Shibata A, Sugiyama Y. 1995. Dynamical model of traffic congestion and numerical simulation. *Physical Review E* 51:1035−42
56. Helbing D, Tilch B. 1998. Generalized force model of traffic dynamics. *Physical Review E* 58:133−38
57. Jiang R, Wu Q, Zhu Z. 2001. Full velocity difference model for a car-following theory. *Physical Review E* 64:017101
58. Sun D, Kang Y, Yang S. 2015. A novel car following model considering average speed of preceding vehicles group. *Physica A: Statistical Mechanics and Its Applications* 436:103−9
59. Kuang H, Yang F, Wang M, Peng G, Li X. 2021. Multi-anticipative average flux effect in the lattice hydrodynamic model. *IEEE Access* 9:35279−86
60. Berg P, Mason A, Woods A. 2000. Continuum approach to car-following models. *Physical Review E* 61:1056−66
61. Fan E. 2000. Extended tanh-function method and its applications to nonlinear equations. *Physics Letters A* 277:212−18
62. Elwakil SA, El-Labany SK, Zahran MA, Sabry R. 2005. Modified extended tanh-function method and its applications to nonlinear equations. *Applied Mathematics and Computation* 161:403−12
63. Jiang R, Wu Q, Zhu Z. 2001. A new dynamics model for traffic flow. *Chinese Science Bulletin* 46:345−48
64. Castillo JMD, Benítez FG. 1995. On the functional form of the speed-density relationship—I: general theory. *Transportation Research Part B: Methodological* 29:373−89
65. Herrmann M, Kerner BS. 1998. Local cluster effect in different traffic flow models. *Physica A: Statistical Mechanics and Its Applications* 255:163−88
66. Kerner BS, Konhäuser P. 1993. Cluster effect in initially homogeneous traffic flow. *Physical Review E* 48:R2335−R2338